BRAIN CONNECTIVITY
Volume 6, Number 6, 2016

DOI: 10.1089/brain.2015.0411

Intrinsic Connectivity Provides the Baseline Framework for Variability in Motor Performance: A Multivariate Fusion Analysis of Low- and High-Frequency Resting-State Oscillations and Antisaccade Performance

Sharna D. Jamadar,[1–3] Gary F. Egan,[1–3] Vince D. Calhoun,[4,5] Beth Johnson,[2] and Joanne Fielding[2,6]

Abstract

Intrinsic brain activity provides the functional framework for the brain's full repertoire of behavioral responses; that is, a common mechanism underlies intrinsic and extrinsic neural activity, with extrinsic activity building upon the underlying baseline intrinsic activity. The generation of a motor movement in response to sensory stimulation is one of the most fundamental functions of the central nervous system. Since saccadic eye movements are among our most stereotyped motor responses, we hypothesized that individual variability in the ability to inhibit a prepotent saccade and make a voluntary antisaccade would be related to individual variability in intrinsic connectivity. Twenty-three individuals completed the antisaccade task and resting-state functional magnetic resonance imaging (fMRI). A multivariate analysis of covariance identified relationships between fMRI oscillations (0.01–0.2 Hz) of resting-state networks determined using high-dimensional independent component analysis and antisaccade performance (latency, error rate). Significant multivariate relationships between antisaccade latency and directional error rate were obtained in independent components across the entire brain. Some of the relationships were obtained in components that overlapped substantially with the task; however, many were obtained in components that showed little overlap with the task. The current results demonstrate that even in the absence of a task, spectral power in regions showing little overlap with task activity predicts an individual's performance on a saccade task.

Key words: antisaccade; functional magnetic resonance imaging (fMRI); intrinsic connectivity; low-frequency oscillations; multivariate covariate analysis; oculomotor; resting-state fMRI; time-course spectra

Introduction

It is becoming increasingly apparent that the intrinsic functional architecture of the brain provides a baseline framework for the individual's full range of extrinsic responses (Fox et al., 2006; Mennes et al., 2011; Raichle, 2010, 2011; Smith et al., 2009). Intrinsic connectivity is typically measured using resting-state blood oxygenation level-dependent functional magnetic resonance imaging (BOLD-fMRI) (Biswal et al., 1995; Cordes et al., 2001; Fox and Raichle, 2007), a robust approach that shows high test–retest reliability (Franco et al., 2013; Shehzad et al., 2009; Zuo et al., 2010b) and a high degree of concordance across participants and testing protocols (Biswal et al., 2010). Several different methods have delineated a large number of reliable and temporally coherent networks that subserve critical functions such as vision, attention, motor planning, and higher-order control (Allen et al., 2011; Calhoun et al., 2001; Laird et al., 2011; Smith et al., 2009). Intrinsic connectivity of resting-state networks shows a high degree of heritability (Fornito et al., 2011; Glahn et al., 2010), and a range of neuropsychiatric and neurodegenerative illnesses are characterized by alterations in

[1]Monash Biomedical Imaging, Monash University, Melbourne, Australia.
[2]Monash Institute of Cognitive and Clinical Neurosciences and School of Psychological Sciences, Monash University, Melbourne, Australia.
[3]Australian Research Council Centre of Excellence for Integrative Brain Function, Monash University, Melbourne, Australia.
[4]The Mind Research Network, Albuquerque, New Mexico.
[5]Department of Electrical and Computer Engineering, University of New Mexico, Albuquerque, New Mexico.
[6]Department of Medicine, University of Melbourne, Melbourne, Australia.

intrinsic networks, including schizophrenia and bipolar disorder (Calhoun et al., 2009, 2012), autism (Kennedy and Courchesne, 2008), affective disorder (Anand et al., 2005), attention-deficit/hyperactivity disorder (Castellanos et al., 2008), and Alzheimer's disease (Li et al., 2002), among others. Individual differences in resting-state connectivity are also linked to individual variability in behavior, from simple motor responses (Duff et al., 2008; Fox et al., 2007) and sensory processing (Ress et al., 2000) to higher-order processes, including working memory (Hampson et al., 2006) and executive control (Mennes et al., 2011). Thus, evidence suggests that resting-state fMRI indexes the intrinsic starting point upon which all other activity is built upon (e.g., for tasks, proactive and reactive behaviors, executively controlled or prepotent responses).

Resting-state networks are characterized by spontaneous large-amplitude low-frequency oscillations that are temporally correlated across functional areas (Allen et al., 2011; Beckmann et al., 2005; Biswal et al., 1995; Cordes et al., 2001; Zuo et al., 2010a). Spontaneous BOLD fluctuations follow a 1/f distribution, with higher power at low frequencies (Zahran et al., 1997). The neural component of functional connectivity is dominated by oscillations within the 0.01–0.1 Hz range, with evidence that oscillations in higher frequencies (>0.1 Hz) index non-neural signals in the neurovasculature and cerebrospinal fluid (Cordes et al., 2001), although some recent studies suggest that higher frequencies may have a neural component (Boubela et al., 2013; Niazy et al., 2011). Low-frequency oscillation power tends to be higher in the gray than the white matter of the cortex (Duff et al., 2008; Zuo et al., 2008, 2010a) and in posterior and medial structures, including visual cortex, posterior cingulate, precuneus, anterior cingulate, and medial prefrontal cortex (Ghosh et al., 2008; Zuo et al., 2008, 2010a).

The presence of a task changes the spatial and temporal dynamics of the intrinsic networks (e.g., Calhoun et al., 2008; Hampson et al., 2006), and low-frequency oscillation power during rest predicts performance and the magnitude of task-related BOLD responses (Fox et al., 2006). This is consistent with the argument that intrinsic and extrinsic BOLD activities share a common underlying mechanism, and that extrinsic activity builds upon baseline intrinsic activity (Fox et al., 2006; Mennes et al., 2011; Raichle, 2010). In this way, individual variability in extrinsic neural and behavioral responses is intimately linked to individual variability in intrinsic neural activity.

The generation of a motor movement in response to sensory stimulation is one of the most fundamental functions of the central nervous system (Munoz et al., 2000). Saccades are rapid eye movements that redirect the visual axes to bring successive visual images onto the fovea (Enderle, 2002). Saccadic eye movements are among the fastest (<100 msec, maximal velocity $\sim$500°/sec) and most stereotyped responses in our behavioral repertoire (Catz and Thier, 2007; Enderle, 2002). Saccadic tracking is complemented by a fixation mechanism that keeps the visual image steady on the fovea for detailed visual analysis. The saccade–fixation process is repeated several hundred thousand times a day and is therefore essential to a variety of sensorimotor behaviors, from reflexive movements toward novel stimuli, to remembered sequences of gaze shifts in the service of task goals (Leigh and Kennard, 2004; Munoz et al., 2000). The generation of any saccade involves a tradeoff between bottom-up signals driven by stimulus properties and top-down signals reflecting current goals and intentions. Saccade parameters are influenced by a range of cognitive processes, from lower-order sensory and perceptual processes to higher-order working memory, attentional, inhibitory, and executive control processes (McDowell et al., 2008). In sum, the saccadic eye movement system can be considered one of the most cardinal behavioral control systems in the brain, at times operating under a high level of automation and, at other times, under a high level of control.

By far, the most common task to investigate saccadic eye movement control is the antisaccade task. A correctly executed *antisaccade* requires subjects to fixate on a central stimulus, which is replaced by a sudden onset target presented peripherally, refrain from looking at the peripheral target, and direct gaze to its mirror image location. Performance on antisaccade trials is usually compared with performance on *prosaccade* trials, which require visually guided shifts of gaze to the sudden onset target. The antisaccade task reliably activates a distributed neural network, encompassing dorsolateral and ventrolateral prefrontal cortices, anterior cingulate, frontal and supplementary eye fields, motor cortex, thalamus, basal ganglia, superior and inferior parietal cortex, occipital cortex, and cerebellum (Jamadar et al., 2013).

Individual variation in the ability to control saccadic eye movements is related to fMRI activity in the frontal eye fields, parietal lobe, basal ganglia, occipital lobe, and cerebellum (Jamadar et al., 2015). Numerous studies have demonstrated that individual differences in the ability to control saccadic eye movements can be predictive of underlying neuropathology. Impairment in saccadic eye movement control as indexed by the antisaccade task is currently under investigation as a biomarker for a range of neuropsychiatric and neurodegenerative illnesses, including schizophrenia (Raemaekers et al., 2002), autism (Luna et al., 2001), affective disorder (Curtis et al., 2001), attention-deficit/hyperactivity disorder (O'Driscoll et al., 2005), and Alzheimer's disease (Shafiq-Antonacci et al., 2003), among others.

Given that saccadic eye movements are (1) often highly automatic under bottom-up sensory conditions, (2) can be placed under executive control given attentional and task constraints, and (3) can be predictive of wider neuropathology, individual differences in the ability to control eye movements may be related to intrinsic connectivity of the brain. While some studies have considered relationships between interindividual variability in intrinsic connectivity and behavior (e.g., Duff et al., 2008; Fox et al., 2007; Mennes et al., 2011), no study to date has examined the relationship between intrinsic connectivity and saccadic eye movement control. This study examines the relationship between interindividual variability in resting-state low-frequency oscillations and saccadic eye movement control, indexed by performance on the antisaccade task.

High-dimensional independent component analysis (ICA) (Allen et al., 2011; Kiviniemi et al., 2009; Smith et al., 2009) was used to examine low-frequency oscillations within functionally discrete regions. The use of high-dimensional ICA instead of a voxel-wise approach gives an increased specificity of links between intrinsic connectivity in functionally discrete regions and saccadic control. The multivariate analytic approach optimizes sensitivity to identify cross-modal relationships (resting-state fMRI, behavior) and reduces unnecessary

testing and hence reliance on multiple comparisons correction (Allen et al., 2011).

Thus, this study aimed to determine if individual variability in the intrinsic connectivity of the brain is related to individual variability in the ability to control saccadic eye movements. It was hypothesized that individual variability in the intrinsic connectivity of regions known to be involved in the control of eye movements would predict an individual's performance on the antisaccade task.

Methods

Participants

Twenty-three healthy individuals (aged 25.8 ± 7.1 years, 11 males) participated in this study. Exclusion criteria included prior exposure to the antisaccade task, current diagnosis of Axis I disorder, first-degree relative with Axis I disorder, history of neurological impairment or head trauma, claustrophobia, nonmagnetic resonance (MR)-compatible implant, and pregnancy in females. All participants had normal or corrected-to-normal vision. Participants were highly educated (17.2 ± 2.8 years of education), showed minimal levels of depression (Beck Depression Inventory M = 4.2, SD = 4.3), and did not currently use tobacco or recreational drugs.

Stimuli and tasks

The task was programmed in Experiment Builder v.10 (SR Research, Ontario Canada). Antisaccade, prosaccade, and null trials were presented in pseudorandomized order (no more than four repetitions of the same task, no runs of consecutive nulls, even number of right and left targets within task, and no more than four consecutive targets in the same hemisphere) across four blocks. Participants completed 96 trials of antisaccade, 96 trials of prosaccade, and 28 (15%) null trials.

The duration of antisaccade and prosaccade trials was fixed at 5500 msec. Each trial began with the presentation of a fixation cross (fixation-1 96 × 96 pixels) on a black background presented for 500, 100, 1500, or 2000 msec randomized between trials.[1] Fixation-1 was removed and followed by a blank screen (200 msec), after which the target (filled circle diameter 96 pixels with 30 × 30 pixel cross hairs in center) appeared on either the left or right side of the screen for 1500 msec. The target was followed by a fixation cross (fixation-2, 96 × 96 pixels) until the end of the trial (duration varied as a function of fixation-1 duration). For antisaccade and prosaccade trials, fixation-1 and the target were colored in one of two cue colors (e.g., magenta = antisaccade, turquoise = prosaccade, or vice versa, counterbalanced between individuals); fixation-2 was always white. Null trials consisted of a white fixation cross, presented 3500 m and visually indistinguishable from fixation-2; thus, participants could not identify when a null trial was in progress.

During resting-state fMRI, participants were instructed to lie quietly in the scanner for 5 min (116 volumes) with eyes open; lights were on in the scanner bore and visual projection turned off.

Procedure

Participants completed a fixed protocol of fMRI of the antisaccade task (24 min), diffusion tensor imaging (DTI, 21 min), resting-state scan (5 min), and structural scan (7 min). In this study, we report the behavioral results obtained during task-based fMRI and resting-state fMRI. The results of the antisaccade task-based fMRI are reported in Jamadar and colleagues (2015).

Data acquisition and analysis

Oculomotor data. Horizontal displacement of the eye was recorded simultaneously with fMRI using an MR-compatible video-based SR Research EyeLink 1000 system, with a spatial resolution of 0.01°degrees and a sampling rate of 500 Hz.

In-house software was used to mark the time and location of target onset and offset, as well as saccade onset and offset. The onset of the saccade was defined as the time when eye velocity exceeded 30° per second; the end of a saccade was defined as the time after saccade onset when eye velocity fell below 10° per second. Each trial was manually inspected to ensure correct placement of target and saccade markers, as well as to screen for any errors. Trials were excluded from further analysis if they exhibited (1) blinks before 100 msec of the target onset or during the primary saccade, (2) unstable or poor fixation on the centrally presented target (±0.5° from center), (3) small saccades with amplitude <3°, or (4) anticipatory eye movements (saccades made within 100 msec of the peripheral target appearing).

Latency of the primary saccade was defined as the time difference between target onset and the primary saccade onset. Directional errors were defined as trials in which a prosaccade was made during an antisaccade trial, or in which an antisaccade was made during a prosaccade trial. The proportion of trials, in which a directional error was made, was calculated for both pro- and antisaccades as the (number of trials with a directional error/total number of trials analyzed) × 100.

MR image data. MR images were acquired on a Siemens Skyra 3T wide-bore scanner with a 32-channel head coil. fMRI during rest was acquired using a T2*-weighted GRAPPA (acceleration factor = 2, partial Fourier = 6/8) echo-planar imaging (EPI) sequence (ascending axial acquisition, 116 volumes, TR = 2.5 sec, TE = 30 msec, FOV = 192 mm, acquisition matrix = 64 × 64, 44 slices, 3 × 3 × 3 mm voxels). Structural magnetic resonance imaging (MRI) was acquired using a T1-weighted 3D MPRAGE sequence (TR = 1900 msec, TE = 2.43 msec, flip angle = 9°, matrix = 192 × 192 m, voxel size = 0.6 × 0.6 × 0.6 mm, 256 slices).

MRI data were analyzed with SPM8 (Wellcome Department of Cognitive Neurology, London). For resting-state fMRI, the first five images were discarded to account for T1 saturation effects. EPI slice acquisition timing differences were corrected using the central slice as reference, realigned to the first nondummy image, and coregistered to their individual structural scans. Structural scans were then segmented using the unified segmentation algorithm in SPM8, which jointly segments and derives parameters to normalize from subject to Montreal Neurological Institute (MNI) space. Functional and structural scans

[1]This manipulation was used to introduce jitter into our design, thereby improving the estimation of the hemodynamic response of individual trials (Dale, 1999). It is possible, however, that this manipulation inadvertently introduced a task difficulty confound; see Ruge and colleagues (2013) for a discussion of such effects.

were then normalized to the MNI template using these parameters and spatially smoothed using a $6\times6\times6$ mm full-width half maximum (FWHM) Gaussian kernel. For all participants, motion was less than a voxel.

Multivariate covariate analysis. Mancovan (v1.0) (Allen et al., 2011), as implemented in GIFT (v3.0a, http://mialab.mrn.org/software/gift), was used to examine relationships between resting-state fMRI time course spectra and antisaccade behavior. Analysis was conducted in three steps: (1) a high-dimensional ICA, (2) identification of resting-state, noise, and mixed-signal networks, and (3) Mancovan of resting-state network time course spectra and behavioral measures.

High-dimensional ICA. Preprocessed images were entered into Group ICA implemented in GIFT (Calhoun and Adali, 2012; Calhoun et al., 2001). Group ICA was conducted in several steps. Subject-specific principal component analysis (PCA) retained 111 principal components (PCs) using standard economy-size decomposition (Erhardt et al., 2011). The PCs for each subject were then concatenated into a single group of 2553 PCs (111 PCs ×23 subjects) and then reduced to 75 independent components (ICs) using the infomax approach (Bell and Sejnowski, 1995); ICA was repeated 20 times using the ICASSO approach to estimate the reliability of decomposition. Individual subject images and time courses were back-reconstructed using the GICA-3 algorithm (Erhardt et al., 2011) and scaled to Z scores. Components averaged across all subjects were calculated with a one-sample *t*-test and thresholded at false discovery rate-corrected $p<0.001$.

Identification of resting-state networks. A subset of ICs were identified as resting-state networks using a combination of visual inspection of aggregate IC spatial maps and objective component metrics, following the approach of Allen and colleagues (2011). Each IC spatial map was rated as a definite/probable artifact, mixed signal, or definite/probable resting-state network based on similarity to previously published high-dimensional ICA (Allen et al., 2011; Kiviniemi et al., 2009) and spatial overlap with known vascular, ventricular, motion, and susceptibility artifacts.

IC spectra were then characterized using two objective metrics of resting-state ICs (Robinson et al., 2009): dynamic range, defined as the difference between the peak power and the minimum power to the right of the peak; and power ratio, defined as the ratio of the integral of spectral power below 0.10 Hz to the integral of power between 0.15 and 0.25 Hz. Dynamic range and power ratio were then plotted against each other (Fig. 1). Previous results have shown that known resting-state networks tend to cluster in the upper right of the spectral features plot and known artifact-related components clustered in the lower left of the plot, with mixed components scattered through the middle (Allen et al., 2011; Robinson et al., 2009). Based on this plot, the categorization of ICs previously listed as probable artifact or resting state was refined as definite artifact or resting-state networks.

Following this systematic categorization, 48 ICs were identified as resting-state networks, 5 as mixed signal, and 22 as artifact. Remaining components showed ICASSO stability $Iq>0.9$.

Mancovan covariate analysis. For full details of the Mancovan approach implemented in GIFT, see Allen et al. (2011). The multivariate selection strategy reported by Allen and colleagues (2011) was used as implemented in Mancovan (v1.0) in the GIFT toolbox (v3.0a) to examine the relationship between resting-state network time course spectra and antisaccade performance. In this approach, multivariate analysis of covariance (MANCOVA) is used to test whether each predictor explains variability in the multivariate response. Significant multivariate results are then followed by pairwise univariate contrasts (corrected for multiple comparisons) to identify regions of the time course spectra that significantly covary with performance.

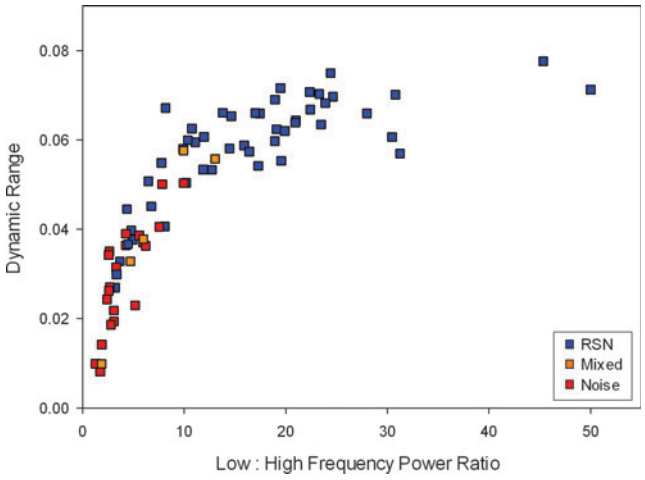

FIG. 1. Scatterplot of dynamic range vs. low-: high-frequency power ratio for IC time course spectra. ICs were categorized as resting-state networks (RSNs, blue), noise (red), or mixed signal (orange) by a combination of visual inspection and spectral characteristics. IC, independent component.

Multivariate analysis involves defining the design matrix, choosing the feature of interest (time course spectra) and reducing dimensionality, and model selection.

The design matrix included the following main effects: antisaccade latency, antisaccade directional error rate, prosaccade latency, and prosaccade directional error rate; and the following interactions: antisaccade latency with directional error rate, prosaccade latency with directional error rate, antisaccade latency with prosaccade latency, and antisaccade directional error rate with prosaccade directional error rate. Rotational and translational movement parameters were included as covariates of no interest. Prosaccade performance and interactions (with antisaccades) were modeled to ensure the results were specific to the cognitive processes involved in antisaccade trials, beyond baseline saccadic processes indexed by prosaccade trials. Directional error rate for both trial types was log transformed to account for the non-normal distribution (both Shapiro–Wilks $p<0.007$). Movement parameters were included as covariates of no interest (nuisance predictors) as Allen and colleagues (2011) showed that it improves estimates for predictors of interest. Nuisance predictors were not strongly associated with covariates of interest (all $p>0.245$).

For the identified resting-state ICs, the time course spectra were estimated on detrended subject-specific time courses using the method implemented in the Mancovan toolbox (v1.0), which implements the multitaper approach of Chronux (http://chronux.org) with the time-bandwidth

product set to three and the number of tapers set to five (Mitra and Bokil, 2008). Individual subject time course spectra were log-transformed, which is useful because it normalizes the highly skewed power distribution, and a response matrix was then formed by concatenation of the subject response vectors. Spectra with 65 frequency bins were reduced to 10 dimensions using PCA.

In model selection, for each of the ICs, the MANCOVA model predicting spectral power was reduced to include only the predictor terms not associated with higher-order interactions ($p < 0.01$) using backward selection, as implemented in mStepwise in the MATLAB (R2011b, The MathWorks) MANCOVAN toolbox (www.mathworks.com/matlabcentral/fileexchange/27014-mancovan).

Following this multivariate analysis, univariate tests were conducted to determine which spectral bins are associated with performance. Univariate models were fit to the original (not dimension-reduced) data to test the association with antisaccade latency and directional error rate. Associations were visualized by plotting the log of the p-value with the sign of the associated t-statistic ($-\text{sign}(t)\log_{10}p$) to provide information of the directionality and statistical strength of the association. Components showing significant relationship with behavior in single nonconsecutive time bins are shown in Figure 5, but are not discussed further.

Results

Behavioral results

Full behavioral results are reported in Jamadar and colleagues (2015), but a summary is presented here for completeness. Behavioral results are shown in Figure 2. Latency and directional error rate data were analyzed with separate two-trial (antisaccade, prosaccade) repeated-measures ANOVA. Antisaccade trials were performed slower ($F(1,22) = 82.21$, $p < 0.001$) and showed a higher directional error rate ($F(1,22) = 12.85$, $p = 0.002$) than prosaccade trials.

fMRI results

The spatial maps of the 48 selected resting-state networks are shown in Figure 3. MNI coordinates, anatomical labels, and T values for the maxima within each IC are shown in Table 1. The identified resting-state networks were compatible with those obtained by previous studies using high-dimensional ICA (Allen et al., 2011; Kiviniemi et al., 2009).

Results for the multivariate covariate analysis are shown in Figure 4 for the behavioral main effects (latency and directional error rate for antisaccade and prosaccade trials), the behavioral interactions (antisaccade latency with antisaccade error, antisaccade latency with prosaccade latency, antisaccade error with prosaccade error, prosaccade latency with prosaccade error), and nuisance predictors (rotation, translation). In this map, ICs are sorted anatomically, then by overlap with antisaccade greater than baseline task fMRI maps from Jamadar and colleagues (2015).

In general, antisaccade performance was related to time course spectra throughout the brain, particularly ICs in frontal, frontoparietal, motor, visual, and cerebellar regions. As can be seen from Figure 4, prosaccade performance main effects and interactions were retained in the final model, supporting the argument that these terms are necessary to improve the estimates of antisaccade performance and time course spectra correlations. Prosaccade performance was related to ICs in frontal, frontoparietal, motor, basal ganglia, and cerebellar regions. Consistent with Allen and colleagues (2011), rotation and translation covariates of no interest were retained in the final model, suggesting that these movement-related parameters are required to improve the estimates of the covariates of interest.

To follow-up the multivariate results, univariate tests on the two performance metrics of most interest, antisaccade latency and directional error rate, were conducted and are shown in Figure 5.

Antisaccade latency was positively related to spectral power in a number of components, including frontal component F4, which showed strongest loadings in bilateral frontopolar cortex; component F6, which has strongest loadings in anterior cingulate; motor component M4, which showed highest loading in right supplementary motor area (supplementary eye fields) and bilateral precentral gyri (frontal eye fields); cerebellar component C1, which showed highest loadings in bilateral cerebellar lobule VI (culmen); component C2, which showed highest loadings in right cerebellar lobule VIII (tonsil); and OC4, which showed highest loadings in the right lingual gyrus.

The antisaccade directional error rate was related to spectral power in component F1, which showed strongest loadings in frontopolar cortex; component F8, which showed strongest loadings in medial frontal gyrus (frontal eye fields); default mode components, DM1 and DM2, which showed strongest loadings in orbitofrontal cortex and posterior cingulate, respectively; component TP1, which showed strongest loadings in bilateral inferior parietal lobule; and occipital components, OC5 and OC6, which showed strongest loadings in bilateral lingual and middle occipital gyri, respectively.

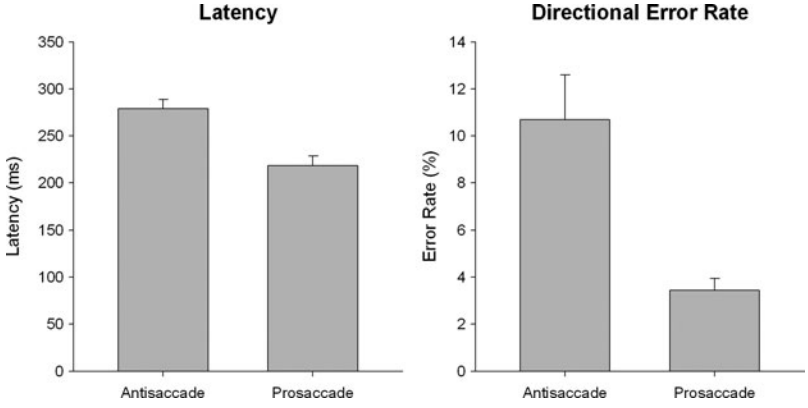

FIG. 2. Antisaccade and prosaccade trial latency (left) and directional error rate (right). Error bars show standard error.

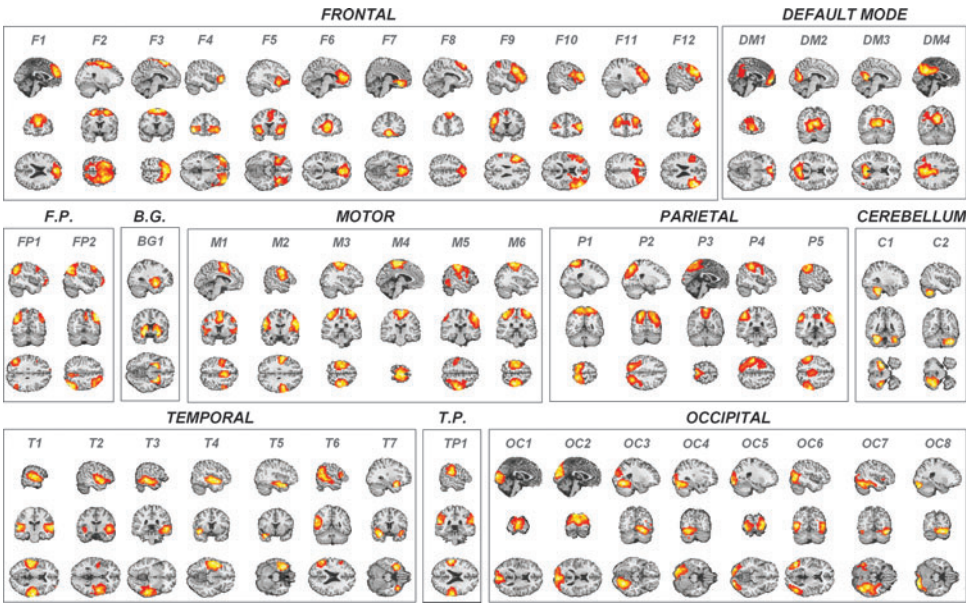

FIG. 3. Forty-eight resting-state networks entered into the Mancovan analysis. ICs were sorted by anatomy, then by overlap with the task activation maps reported by Jamadar and colleagues (2015). Components are labeled according to their anatomical location (e.g., Frontal, Parietal), then ranked by overlap with task activation map. See Table 1 for MNI coordinates of maxima and *T* values for each IC. B.G., basal ganglia; C, cerebellum; DM, default mode; F, frontal; F.P., frontoparietal; M, motor; OC, occipital; P, parietal; T, temporal; T.P., temporoparietal.

Discussion

Behavior–intrinsic connectivity relationships

Significant multivariate relationships between antisaccade latency and directional error rate were obtained in independent components across the entire brain. While some of the significant relationships were obtained in components that overlapped substantially with the known ocular motor network (e.g., frontal, motor, and cerebellar ICs), many were obtained in components that show little overlap with the ocular motor network (e.g., temporal ICs). This is consistent with a previous study by Baria and colleagues (2011) who showed that frequency-specific energy changes in resting-state networks in the presence of a task often occur outside of regions explicitly involved in the task. In other words, in the presence of a task, global and local energies are exchanged between frequency bands in a widespread network of regions that may or may not overlap with the task.

Follow-up univariate analyses showed that antisaccade latency was related to intrinsic fluctuations in a number of regions, including frontopolar cortex, anterior cingulate, supplementary eye fields, lingual gyrus, and cerebellar lobules VI and VIII. Directional error rate was related to intrinsic fluctuations across multiple components spanning frontopolar cortex, frontal eye fields, default mode regions, and visual areas. Importantly, our results suggest that increased high-frequency fluctuations in these regions are associated with more cautious performance—that is, increased spectral high-frequency spectral power is associated with both increased antisaccade latency and decreased error rate, consistent with a speed–accuracy tradeoff. Thus, an individual's intrinsic high-frequency spectral power may be predictive of the level of caution exerted when performing a cognitively demanding task.

A number of the regions found to be related to antisaccade behavior are highly implicated in the ocular motor network that is engaged during the antisaccade task, including the anterior cingulate, frontal and supplementary eye fields, and cerebellum (Jamadar et al., 2013, 2015). The anterior cingulate is important for conflict and error monitoring on interference-prone antisaccade trials, eliciting a signal for greater cognitive control in high interference contexts (Ford et al., 2005). The frontal and supplementary eye fields are important for the preparation of the voluntary saccade (Pierrot-Deseilligny et al., 2004), with the supplementary eye field particularly involved in initiating the signal to inhibit the prepotent prosaccade response (Schlag-Rey et al., 1994). The two cerebellar components appear to overlap substantially with the hemispheric ocular motor region discussed by Prsa and Thier (2013), which is involved in the cognitive control of eye movements. Relationships between the intrinsic connectivity of the frontopolar cortex and behavior are consistent with this region's role in higher-order cognitive control. This region is believed to play a role in branching control, allowing an ongoing task to be interrupted and maintained in a pending state while another is being performed and to be quickly returned to after the intermediate task is completed (Koechlin and Summerfield, 2007). In the current context, the latency and accuracy of the antisaccade may therefore be related to the effectiveness of the individual's ability to pause the prepotent prosaccade response until the antisaccade task requirement is completed.

Thus, many of our brain–behavior relationships were obtained in regions involved in cognitive control and reducing conflict and interference. Most models of antisaccade performance postulate that inhibition of the prepotent prosaccade response is critical for successful performance of an antisaccade (e.g., Everling and Fischer, 1998; Isoda and Hikosaka, 2011; Massen, 2004; Munoz and Everling, 2004). In classic serial models of the antisaccade task, increased latency for antisaccade compared with prosaccade trials is due to the requirement to inhibit the prepotent prosaccade response and inversion of the target location into a voluntary motor command to look away from the target (Everling and Fischer, 1998). In more recent competition-based models, at target onset, there is competition between the prepotent prosaccade response and goal-directed antisaccade response—if the antisaccade response is computed fast enough, it reaches

Table 1. MNI Coordinates, Anatomical Labels, Brodmann Areas, and *T* Values for the Maxima in Each Independent Component

IC #	*Maxima MNI*	*Maxima label*	*BAs*	T *max*
Frontal				
F1	0, 47, 22	Superior medial frontal gyrus	9, 8, 10	24.06
F2	−24, 5, 58	L superior frontal gyrus	6, 8, 7, 4, 3	20.87
F3	6, 11, 64	R superior frontal gyrus	6	18.45
F4	−45, 44, −2	L middle frontal gyrus	10	17.47
F5	36, 17, −14	R inferior frontal gyrus	47, 32	26.69
F6	6, 44, 13	R anterior cingulate	10, 32, 9, 24	25.68
F7	−6, 32, −11	L orbitofrontal gyrus	11	23.33
F8	9, 41, 52	R superior medial frontal gyrus	8, 6	29.29
F9	−45, 11, 28	L inferior frontal gyrus	9, 47, 45, 40, 8	20.78
F10	48, 35, 16	R inferior frontal gyrus	10, 46, 45	19.69
F11	−27, 38, 40	L middle frontal gyrus	10, 9, 32, 8	21.87
F12	51, 32, 25	R middle frontal gyrus	9, 46	20.76
Default mode				
DM1	−3, 56, −8	L orbitofrontal gyrus	10, 31	25.57
DM2	6, −67, 13	R posterior cingulate	18, 19, 31, 30, 7	25.91
DM3	6, −58, 10	R posterior cingulate	31, 30	21.35
DM4	0, −55, 31	Posterior cingulate/precuneus	7, 31	23.51
Frontoparietal				
FP1	−45, −64, 31	L angular gyrus	7, 40, 39, 31, 10, 8	25.70
FP2	42, −67, 46	R angular gyrus	40, 39, 7, 8, 10, 9	19.14
Motor				
M1	6, 8, 49	R supplementary motor area	6, 32, 24	19.16
M2	−57, −4, 31	L precentral gyrus	6, 4, 3	19.51
M3	36, −31, 64	R precentral gyrus	6, 4, 3	19.82
M4	3, −22, 76	R supplementary motor area	6, 4, 5	21.43
M5	51, −25, 52	R precentral/postcentral gyrus	40, 6, 4, 3, 2	21.81
M6	36, −31, 64	R precentral gyrus	40	19.85
Basal ganglia				
BG1	30, 5, −11	R putamen		17.97
Parietal				
P1	36, 17, −14	R superior parietal lobule	7, 5, 3	22.26
P2	−21, −73, 43	L superior parietal lobule	7, 19, 40	24.89
P3	0, −55, 70	Precuneus	7	29.82
P4	−45, −34, 52	L inferior parietal lobule	40, 6, 7	23.98
P5	54, −37, 49	R inferior parietal lobule	40, 31	22.51
Cerebellum				
C1	−30, −43, −38	L cerebellum lobule VI/culmen		13.42
C2	42, −55, −38	R cerebellum lobule VIII/tonsil		19.36
Temporal				
T1	60, −19, 10	R superior temporal gyrus	22, 13	19.83
T2	48, −7, 1	R superior temporal gyrus	22, 13	22.95
T3	54, −34, −5	R middle temporal gyrus	21, 22, 20	19.97
T4	−48, 8, −11	L superior temporal gyrus	22	15.70
T5	−39, 14, −26	L superior temporal pole	21, 38	19.17
T6	−57, −52, 22	L middle temporal gyrus	22, 40, 39	21.69
T7	−33, 8, −23	L superior temporal pole	38	20.25
Temporoparietal				
TP1	−57, −34, 22	L inferior parietal lobule	40, 6, 4, 3	20.41
Occipital				
OC1	0, −94, 13	Cuneus	18, 17, 19	26.33
OC2	0, −88, 16	Cuneus	19, 18, 17	21.61
OC3	24, −64, −14	R fusiform gyrus	19, 18	17.16
OC4	−33, −73, −23	L lingual gyrus/declive	19, 18	18.22
OC5	21, −91, −11	L lingual gyrus	18, 19, 17	21.19
OC6	−45, −64, 7	L middle occipital/temporal gyrus	19, 37	20.31
OC7	42, −64, −20	R fusiform gyrus	37, 19	19.08
OC8	21, −82, −23	R lingual gyrus/declive	18	13.43

MNI, Montreal Neurological Institute; BAs, Brodmann areas; IC #, independent component number.

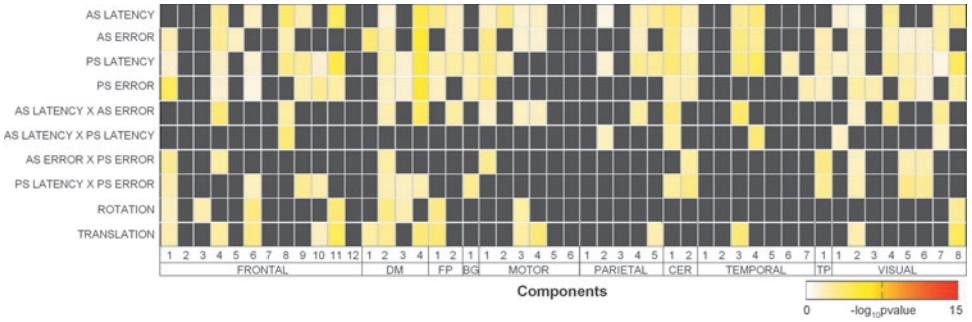

FIG. 4. Multivariate results from the reduced MANCOVA model showing the significance of covariates and their interactions for time course spectra. Gray cells indicate terms that were removed from the full model during backward selection. See Figure 3 for component maps and Table 1 for component MNI coordinates and anatomical labels. AS, antisaccade; CER, cerebellum; PS, prosaccade; MANCOVA, multivariate analysis of covariance.

threshold and is executed. However, if the prosaccade response reaches threshold quicker than the antisaccade response, an erroneous prosaccade response is elicited. Thus, in these models, an inhibitory process is critical to ensure the antisaccade response reaches threshold before the prosaccade response (Isoda and Hikosaka, 2011; Munoz and Everling, 2004). Thus, the current finding that resting-state oscillations in regions involved in cognitive control and inhibiting a response are related to antisaccade latency and error rate suggests that individual variability in the intrinsic connectivity state of these regions predicts an individual's cautiousness in performing a goal-directed task in a high interference context.

Both antisaccade latency and directional error rate were also related to intrinsic connectivity in higher visual cortex (lingual gyrus). While not usually considered an oculomotor or antisaccade region, the lingual gyrus is consistently activated in the antisaccade task during both antisaccade and prosaccade trials (Jamadar et al., 2013). The lingual gyrus is traditionally linked to color processing and knowledge (Chao and Martin, 1999; Miceli et al., 2001; including intrinsic connectivity of the region, Wang et al., 2013), and given that in the present paradigm the currently relevant task (antisaccade/prosaccade) was cued by color cues, it appears straightforward to conclude that color processing of the cue accounts for these results. However, a number of factors lead us to argue that the lingual gyrus may play an important, as yet unappreciated, role in antisaccade task performance, including (1) the consistency of activation of the lingual gyrus across multiple studies and paradigm designs (reviewed in Jamadar et al., 2013); (2) our recent finding that lingual gyrus shows increased fMRI activity following antisaccade training, and that training-related neural changes in the lingual

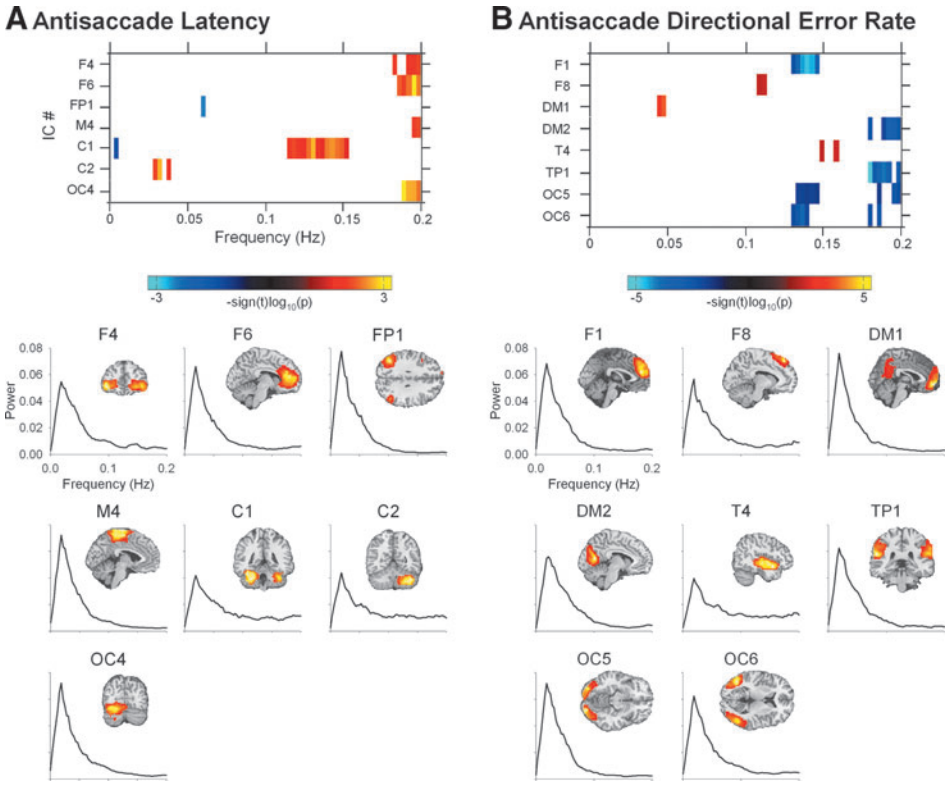

FIG. 5. **(A)** Univariate results for the components that showed a significant relationship with antisaccade latency (left) and antisaccade directional error rate (right). **(B)** Time course spectra and component maps for ICs that showed significant univariate relationship with antisaccade latency and directional error rate. IC #, independent component number.

gyrus are associated with training-related changes in performance (Jamadar et al., 2015); and (3) our current finding that increased intrinsic connectivity in this region is associated with better performance (faster latency, reduced error rate). It has been proposed that the lingual gyrus is involved in establishing a representation of visual stimuli for the use of orientation (Aguirre et al., 1998) and with learning of visuospatial and visuomotor contingencies (Nemmi et al., 2013). Total bilateral infarction of the lingual gyri leads to bilateral altitudinal hemianopia (defective vision in upper or lower visual hemifields) and selectively impairs visuospatial and visuomotor learning, with no impairment on color processing, visually guided reaching, or visual smooth pursuit (Bogousslavsky et al., 1987). We argue that the lingual gyrus may be involved in the transformation between the visual input and the required motor response. In most models of the antisaccade task, the process of vector inversion—the translation of the visual location of the target to the mirror image location—is localized to the intraparietal sulcus (Brown et al., 2006; Medendorp et al., 2005; Pierrot-Deseilligny et al., 2004). We argue that the lingual gyrus may play an important role in the visuospatial aspects of the inversion, particularly those related to mapping the orientation of the target. This information may then be parsed to the nearby intraparietal sulcus for the process of inverting this visuospatial information to the mirror image location for the required motor response.

High-dimensional resting-state networks

A high-dimensional ICA was used to extract independent components that index functionally discrete regions of the brain. This approach was adopted to increase the spatial specificity of links between behavior and intrinsic connectivity. While the traditional approach to resting-state fMRI analysis is to estimate a low model order (number of ICs $\sim$20; see Laird et al., 2011 for a review), it is becoming increasingly recognized that the resulting components represent the summation of multiple subcomponents (Kiviniemi et al., 2009) that may show quite distinct patterns of neural activity (Baria et al., 2011). Higher model order decomposition of resting-state fMRI has been shown to yield refined components that correspond to known anatomical and functional segmentations (Allen et al., 2011; Kiviniemi et al., 2009; Smith et al., 2009).

The high-dimensional ICA yielded 48 resting-state networks, an order of magnitude similar to previous studies (Balsters et al., 2013; Kiviniemi et al., 2009; Smith et al., 2009; but see Allen and colleagues [2011] who used a more stringent network selection criterion). Consistent with previous reports, these resting-state networks together covered almost the entire brain, excluding regions close to regions of known vascular, ventricular, and susceptibility artifacts. Power spectra of the resting-state networks showed the expected 1/f distribution (Zahran et al., 1997) with highest amplitude power in low frequencies, and diminishing power in high frequencies (see Figure 5B for representative power spectra plots).

The strength of the high-dimensional ICA is that one can detect different relationships between individual constituents of a network and behavior. For example, DM1 and DM2 components showed different relationships with antisaccade error rate: for DM1, greater low-frequency power was associated with higher antisaccade error rate, whereas for DM2, greater high-frequency power was associated with reduced antisaccade error rate. Thus, poorer performance in the antisaccade task is related to *greater* low-frequency connectivity in the orbitofrontal-medial posterior cingulate DMN network and *less* high-frequency connectivity in the right posterior cingulate DMN network. This suggests that both low- and high-frequency power within the same network can have distinguishable effects on behavioral performance.

Implications or models of intrinsic connectivity and saccadic control

The current findings add to and extend the literature linking variability in intrinsic connectivity to variability in task performance and fMRI activation (Duff et al., 2008; Fox et al., 2007; Hampson et al., 2006; Mennes et al., 2011). Performance on the antisaccade task was related to intrinsic connectivity in a broad range of regions, some that showed little overlap with task activation maps (multivariate analysis; Figure 4). This extends the recent findings of Baria and colleagues (2011) who showed that in the presence of a task, local and global spectral power changed primarily in regions not activated by the task, shifting the energy profile from low frequency to higher frequency bands. They found that power in the 0.05–0.1 and 0.10–0.15 Hz ranges was most affected by this shifting profile—the bands in which many of the univariate behavior–intrinsic connectivity relationships were found. The current results extend this finding to show that even in the absence of a task, spectral power within these bands and in regions showing little overlap with task activity predicts task performance.

In sum, the current results are consistent with models that posit that intrinsic brain activity provides the baseline for the individual's range of extrinsic behavioral responses (Fox et al., 2006; Mennes et al., 2011; Raichle, 2010). Together with the results of Baria and colleagues (2011), the results show that the baseline neural framework for behavior extends outside of the task-related network, and this extended framework is predictive of task-related behavior. While the current results can only show that the intrinsic connectivity baseline predicts task performance on the antisaccade task, it is likely that the baseline connectivity predicts behavior on most cognitive tasks.

Notably, antisaccade latency and error rate were related to medium- to high-frequency power in a number of components. High-frequency power was related to increased latency and decreased error rate in frontopolar cortex, anterior cingulate, frontal and supplementary eye fields, and lingual gyrus—suggesting that high-frequency power in this component contributes to individual differences in speed–accuracy tradeoff. Resting-state networks are usually characterized as *low-frequency oscillations*, and it is commonly held that the neural sources of BOLD signal fluctuations occur below 0.1 Hz, with cardiac, respiratory, and other sources of signal fluctuation occurring above this frequency (Cordes et al., 2001). Recent evidence suggests, however, that neural sources can be identified in oscillations higher than the traditional 0.1 Hz cutoff (Baria et al., 2011; Boubela et al., 2013; Niazy et al., 2011; Zuo et al., 2010a). Baria and colleagues (2011) showed both global and local changes in low-frequency (0.01–0.1 Hz) and high-frequency (0.1–0.2 Hz) power in the presence of a task. A recent study by Balsters and colleagues (2013) using

the Mancovan approach showed that low-frequency power (in networks that both overlapped or did not overlap with the task) was related to better working memory performance, whereas higher frequency power was related to worse performance. They speculated that an increase in higher frequency oscillations might be indicative of reduced connectivity within the functional network. Such a clear dissociation was not obtained here. Power in the 0.1–0.2 Hz range was related to more cautious performance (slower latency and reduced error rate), suggesting that connectivity within this range may contribute to individual differences in speed–accuracy tradeoff rather than a clear reduction in performance as suggested by Balsters and colleagues (2013). The current results add to this growing body of literature that suggests that higher frequency oscillations >0.10 Hz contribute to behavioral and task activation variability.

The current results also have implications for models of saccade control, suggesting that individual variability in the ability to control eye movements is related to the individual's intrinsic level of activity both within and outside of the traditional oculomotor network. As noted in the Introduction section, many conditions are characterized by a deficit in oculomotor control, including schizophrenia (Raemaekers et al., 2002), attention-deficit/hyperactivity disorder (O'Driscoll et al., 2005), multiple sclerosis (Fielding et al., 2009), and Huntington's disease (Lasker and Zee, 1997), among others. Given that many of these illnesses are also characterized by changes in intrinsic connectivity (schizophrenia: Calhoun et al., 2009; attention-deficit/hyperactivity disorder: Castellanos et al., 2008; multiple sclerosis: Bonavita et al., 2011; Huntington's disease: Werner et al., 2014), it is possible that antisaccade performance and activation differences between neuropsychiatric/neurodegenerative groups and healthy controls are due to the underlying differences in intrinsic connectivity between groups rather than a specific impairment in oculomotor control *per se*. That is, if a group has a lower baseline activity or starting point than healthy controls, then expending a similar level of effort or energy when performing the task will result in lower activation levels and performance. Future studies should explore whether the differences in oculomotor control seen in neuropsychiatric/neurodegenerative groups are distinguishable from intrinsic connectivity differences.

Limitations and conclusions

The current study demonstrated that individual differences in intrinsic connectivity are related to individual differences in antisaccade task performance. The primary limitation of the study is that physiological data were not recorded concurrently with resting-state fMRI. To clearly rule out the possibility that oscillations >0.1 Hz are related to artifactual sources, it is necessary to record physiological data of cardiac and respiratory signals. We believe that a number of these sources would have been removed during the rigorous resting-state component selection (which included visual inspection and a measure of dynamic power vs. low- to high-frequency power ratio) and therefore variance related to non-neural signals should have been minimized. In addition, we note the growing number of studies reporting neural signals in frequencies >0.1 Hz (Allen et al., 2011; Baria et al., 2011; Boubela et al., 2013; Niazy et al., 2011; Zuo et al., 2010a). Nonetheless, in the absence of physiological recordings, the possibility cannot be ruled out that the relationship obtained between latency/error rate and high-frequency power is related to non-neural signals.

A second potential limitation of the current study is that all participants completed the resting-state fMRI scan after the task fMRI scan. For all participants, resting-state fMRI acquisition occurred after a DTI acquisition; that is, at least 21 min after the task fMRI acquisition. Previous studies have shown that the connectivity properties of intrinsic networks are altered in the period immediately following a cognitive task (Barnes et al., 2009; Duff et al., 2008; Waites et al., 2005). However, since Barnes and colleagues (2009) found that resting-state connectivity returned to baseline (i.e., nonsignificantly different from resting-state connectivity measured before task performance) by around 6 min post-task, we believe that contamination of resting-state connectivity measures from previous task performance in the current study is negligible.

It should also be noted that due to the use of high-dimensional ICA, this study is primarily examining intrinsic connectivity at a *local* level rather than at the *network* level, as is possible with low-dimensional ICA. We chose to use a high-dimensional ICA to increase the specificity of the behavior–intrinsic connectivity relationships within functionally defined regions. Network-level relationships as predicted by low-dimensional ICA can be obtained from high-dimensional ICA by analyzing the functional network connectivity of higher-model ICA (Jafri et al., 2008). Future studies may wish to examine how individual differences in intrinsic connectivity at the network level contribute to saccade control.

In sum, the current results are consistent with the argument that intrinsic brain activity provides the functional framework for the brain's full behavioral repertoire (Fox et al., 2006; Mennes et al., 2011; Raichle, 2010) and may contribute to individual differences in speed–accuracy tradeoff of eye movements. Saccadic eye movements in response to a visual target are one of the most cardinal and stereotyped responses in our behavioral repertoire (Munoz et al., 2000), and individual differences in the control of saccadic eye movement are related to individual differences in intrinsic connectivity, both within regions involved in the task and in regions not directly involved in the task.

Acknowledgments

The authors would like to thank Mr. Richard McIntyre and the staff at Monash Biomedical Imaging for assistance with MRI data acquisition. The authors also thank Meaghan Clough for assistance with analysis of the ocular motor data. This work was supported by an Australian Research Council Discovery Grant DP110102084 (J.F. and G.F.E.) and the Australian Research Council Centre of Excellence for Integrative Brain Function (CE140100007). S.D.J. is supported by an Australian Research Council Discovery Early Career Researcher Award DE150100406. G.F.E. is a National Health and Medical Research Committee Principal Research Fellow. V.D.C. is supported by NIH P20GM103472, R01EB005846; NSF 1539067.

Author Disclosure Statement

No competing financial interests exist.

References

Aguirre GK, Zarahn E, D'Esposito M. 1998. An area within human ventral cortex sensitive to ''building'' stimuli: evidence and implications. Neuron 21:373–383.

Allen EA, Erhardt EB, Damaraju E, Gruner W, Segall JM, Silva RF, et al. 2011. A baseline for the multivariate comparison of resting-state networks. Front Syst Neurosci 5:2.

Anand A, Li Y, Wang Y, Wu J, Gao S, Bukhari L, et al. 2005. Activity and connectivity of brain mood regulating circuit in depression: a functional magnetic resonance study. Biol Psychiatry 57:1079–1088.

Balsters JH, Robertson IH, Calhoun VD. 2013. BOLD frequency power indexes working memory performance. Front Hum Neurosci 7:207.

Baria AT, Baliki MN, Parrish T, Apkarian AV. 2011. Anatomical and functional assemblies of brain BOLD oscillations. J Neurosci 31:7910–7919.

Barnes A, Bullmore ET, Suckling J. 2009. Endogenous human brain dynamics recover slowly following cognitive effort. PLoS One 48:e6626.

Beckmann CF, LeLuca M, Devlin JT, Smith SM. 2005. Investigations into resting-state connectivity using independent component analysis. Philos Trans R Soc Lond B Biol Sci 360:1001–1013.

Bell AJ, Sejnowski TJ. 1995. An information maximization approach to blind separation and blind deconvolution. Neural Comput 7:1129–1159.

Biswal B, Yetkin FZ, Haughton VM, Hyde JS. 1995. Functional connectivity in the motor cortex of the resting human brain using echo-planar MRI. Magn Reson Med 34:537–541.

Biswal BB, Mennes M, Zuo XN, Gohel S, Kelly C, Smith SM, et al. 2010. Toward discovery science of human brain function. Proc Natl Acad Sci USA 107:4734–4739.

Bogousslavsky J, Miklossy J, Deruaz J-P, Assal G, Regli F. 1987. Lingual and fusiform gyri in visual processing: a clinic-pathologic study of superior altitudinal hemianopia. J Neurol Neurosurg Psychiatry 50:607–614.

Bonavita S, Gallo A, Sacco R, Corte MD, Bisecco A, Docimo R, et al. 2011. Distributed changes in default mode resting-state connectivity in multiple sclerosis. Mult Scler 17: 411–422.

Boubela RN, Kalcher K, Huf W, Kronnerwetter C, Filzmoser P, Moser E. 2013. Beyond noise: using temporal ICA to extract meaningful information from high-frequency fMRI signal fluctuations during rest. Fron Hum Neurosci 7:168.

Brown MRG, Goltz, HC, Vilis T, Ford K, Everling S. 2006. Inhibition and generation of saccades: rapid event-related fMRI of prosaccades, antisaccades and no-go trials. Neuroimage 33:644–659.

Calhoun VD, Adali T. 2012. Multisubject independent component analysis of fMRI: a decade of intrinsic networks, default mode and neurodiagnostic discovery. IEEE Rev Biomed Eng 5:60–73.

Calhoun VD, Adali T, Pearlson GD, Pekar JJ. 2001. A method for making group inferences from functional MRI data using independent component analysis. Hum Brain Mapp 14:140–151.

Calhoun VD, Eichle T, Pearlson GD. 2009. Functional brain networks in schizophrenia: a review. Front Hum Neurosci 3:17.

Calhoun VD, Kiehl KA, Pearlson GD. 2008. Modulation of temporally coherent brain networks estimated using ICA at rest and during cognitive tasks. Hum Brain Mapp 29:828–838.

Calhoun VD, Sui J, Kiehl K, Turner J, Allen E, Pearlson GD. 2012. Exploring the psychosis functional connectome: aberrant intrinsic networks in schizophrenia and bipolar disorder. Front Psychiatry 2:75.

Castellanos FX, Margulies DS, Kelly C, Uddin LQ, Ghaffari M, Kirsch A, et al. 2008. Cingulate-precuneus interactions: a new locus of dysfunction in adult attention-deficit/hyperactivity disorder. Biol Psychiatry 63:332–337.

Catz N, Thier P. 2007. Neural control of saccadic eye movements. Dev Ophthalmol 40:52–75.

Chao LL, Martin A. 1999. Cortical regions associated with perceiving, naming and knowing about colors. J Cogn Neurosci 11:25–35.

Cordes D, Haughton VM, Arfanakis K, Carew JD, Turski PA, Moritz CH, et al. 2001. Frequencies contributing to functional connectivity in the cerebral cortex in ''resting-state'' data. AJNR Am J Neuroradiol 22:1326–1333.

Curtis CE, Calkins ME, Grove WM, Feil KJ, Iacono WG. 2001. Saccadic disinhibition in patients with acute and remitted schizophrenia and their first-degree biological relatives. Am J Psychiatry 158:100–106.

Dale A. 1999. Optimal experimental design for event-related fMRI. Hum Brain Mapp 8:109–114.

Duff EP, Johnston LA, Xiong K, Fox PT, Mareels I, Egan GF. 2008. The power of spectral density analysis for mapping endogenous BOLD signal fluctuations. Hum Brain Mapp 29:778–790.

Enderle JD. 2002. Neural control of saccades. Prog Brain Res 140:21–49.

Erhardt EB, Rachakonda S, Bedrick EK, Allen EA, Adali T, Calhoun VD. 2011. Comparison of multi-subject ICA methods for analysis of fMRI data. Hum Brain Mapp 32: 2075–2095.

Everling S, Fischer B. 1998. The antisaccade: a review of basic research and clinical studies. Neuropsychologia 36:885–899.

Fielding J, Kilpatric T, Millist L, White O. 2009. Antisaccade performance in patients with multiple sclerosis. Cortex 45: 900–903.

Ford KA, Goltz HC, Brown MRG, Everling S. 2005. Neural processes associated with antisaccade task performance investigated with event-related fMRI. J Neurophysiol 94: 429–440.

Fornito A, Zalesky A, Bassett DS, Meunier D, Ellison-Wright I, Yucel, M, et al. 2011. Genetic influences on cost-efficient organisation of human cortical functional networks. J Neurosci 31:3261–3270.

Fox MD, Raichle ME. 2007. Spontaneous fluctuations in brain activity observed with functional magnetic resonance imaging. Nat Rev Neurosci 8:700–711.

Fox MD, Snyder AZ, Vincent JL, Raichle ME. 2007. Intrinsic fluctuations within cortical systems account for intertribal variability in human behaviour. Neuron 56:171–184.

Fox MD, Snyder AZ, Zacks JM, Raichle ME. 2006. Coherent spontaneous activity accounts for trial-to-trial variability in human evoked brain responses. Nat Neurosci 9:23–25.

Franco AR, Mannell M, Calhoun VD, Mayer A. 2013. Impact of analysis methods on the reproducibility and reliability of resting-state networks. Brain Connect 3:363–374.

Ghosh A, Rho Y, McIntosh AR, Kotter R, Jirsa VK. 2008. Noise during rest enables the exploration of the brain's dynamic repertoire. PLoS Comput Biol 4:e1000196.

Glahn DC, Winkler AM, Kochunov P, Almasy L, Duggirala R, Carless MA, et al. 2010. Genetic control over the resting brain. Proc Natl Acad Sci USA 107:1223–1228.

Hampson M, Driesen NR, Skudlarski P, Gore JC, Constable RT. 2006. Brain connectivity related to working memory performance. J Neurosci 26:13338–13343.

Isoda M, Hikosaka O. 2011. Cortico-basal ganglia mechanisms for overcoming innate, habitual and motivational behaviors. Eur J Neurosci 33:2058–2069.

Jafri MJ, Pearlson GD, Stevens M, Calhoun VD. 2008. A method for functional network connectivity among spatially independent resting-state components and schizophrenia. Neuroimage 39:1666–1681.

Jamadar SD, Fielding J, Egan GF. 2013. Quantitative meta-analysis of fMRI and PET studies reveals consistent activation in fronto-striatal-parietal regions and cerebellum during antisaccades and prosaccades. Front Psychol 4:749.

Jamadar SD, Johnson B, Clough, M, Egan GF, Fielding J 2015. Behavioural and neural plasticity of ocular motor control: changes in performance and fMRI activity following antisaccade training. Front Hum Neurosci 9:653.

Kennedy DP, Courchesne E. 2008. The intrinsic functional organization of the brain is altered in autism. Neuroimage 39: 1877–1885.

Kiviniemi V, Starck T, Remes J, Long X, Nikkinen J, Haapea M, et al. 2009. Functional segmentation of the brain cortex using high model order group PICA. Hum Brain Mapp 30: 3865–3886.

Koechlin E, Summerfield C. 2007. An information theoretical approach to prefrontal executive function. Trends Cogn Sci 11:229–235.

Laird AR, Fox PM, Eickhoff SB, Turner JA, Ray KL, McKay DR, et al. 2011. Behavioral interpretations of intrinsic connectivity networks. J Cogn Neurosci 23:4022–4037.

Lasker AG, Zee DS. 1997. Ocular motor abnormalities in Huntington's disease. Vis Res 37:3639–3645.

Leigh RJ, Kennard C. 2004. Using saccades as a research tool in the clinical neurosciences. Brain 127:460–477.

Li SJ, Li Z, Wu G, Zhang MJ, Franczak M, Antuono PG. 2002. Alzheimer disease: evaluation of a functional MR imaging index as a marker. Radiology 225:253–259.

Luna B, Minshew NJ, Garver KE, Lazar NA, Thulbron KR, Eddy WF, Sweeney JA. 2001. Neocortical system abnormalities in autism: an fMRI study of spatial working memory. Neurology 59:834–840.

Massen C. 2004. Parallel programming of exogenous and endogenous components in the antisaccade task. Q J Exp Psychol A 57:475–498.

McDowell JE, Dyckman KA, Austin BP, Clementz BA. 2008. Neurophysiology and neuroanatomy of reflexive and volitional saccades: evidence from studies of humans. Brain Cogn 68:255–270.

Medendorp WP, Goltz HC, Vilis T. 2005. Remapping the remembered target location for antisaccades in the human posterior parietal cortex. J Neurophysiol 94:737–740.

Mennes M, Zuo X-N, Kelly C, Di Martino A, Zang Y-Y, Biswal B, et al. 2011. Linking inter-individual differences in neural activation and behavior to intrinsic brain dynamics. NeuroImage 54:2950–2959.

Miceli G, Fouch E, Capasso R, Shelton JR, Tomaiuolo F, Caramazza A. 2001. The dissociation of colour from form and function knowledge. Nat Neurosci 4:662–667.

Mitra P, Bokhil H. 2008. *Observed Brain Dynamics*. New York: Oxford University Press.

Munoz DP, Dorris MC, Pare M, Everling S. 2000. On your mark, get set: brainstem circuitry underlying saccadic initiation. Can J Physiol Pharmacol 78:934–944.

Munoz DP, Everling S. 2004. Look away: the antisaccade task and the voluntary control of eye movement. Nat Rev Neurosci 5:218–228.

Nemmi F, Boccia M, Piccardi L, Galati G, Guariglia C. 2013. Segregation of neural circuits involved in spatial learning in reaching and navigational space. Neuropsychologia 51: 1561–1570.

Niazy RK, Xie J, Miller K, Beckmann CF, Smith SM. 2011. Spectral characteristics of resting state networks. Prog Brain Res 193:259–276.

O'Driscoll GA, Depatie L, Holahan AL, Savion-Lemieux T, Barr RG, Jolicoeur C, Douglas VI. 2005. Executive functions and methylphenidate response in subtypes of attention-deficit/hyperactivity disorder. Biol Psychiatry 57:1452–1460.

Pierrot-Deseilligny, C, Milea D, Muri RM. 2004. Eye movement control by the cerebral cortex. Curr Opin Neurol 17:17–25.

Prsa M, Thier P. 2013. The cerebellum: eye movements. In: Pfaff DW (ed). *Neuroscience in the 21st Century*. New York, NY: Springer Science.

Raemaekers M, Jansma JM, Cahn W, van der Geest JM, van der Linden JA, Kahn RS, Ramsey NF. 2002. Neuronal substrate of the saccadic inhibition deficit in schizophrenia investigated with 3-dimensional event-related functional magnetic resonance imaging. Arch Gen Psychiatry 59:313–320.

Raichle ME. 2010. Two views of brain function. Trends Cog Sci 14:180–190.

Raichle ME. 2011. The restless brain. Brain Connect 1:3–12.

Ress D, Backus BT, Heeger DJ. 2000. Activity in primary visual cortex predicts performance in a visual detection task. Nat Neurosci 3:940–945.

Robinson S, Basso G, Soldati N, Sailer U, Jovicich J, Bruzzone L, Kryspin-Exner I, Bauer H, Moser E. 2009. A resting state network in the motor control circuit of the basal ganglia. BMC Neurosci 10:1–14.

Ruge, H., Jamadar, S., Zimmerman, U., Karayanidis, F. 2013. The many faces of preparatory control in task-switching: reviewing a decade of fMRI research. Hum Brain Mapp 34:12–35.

Schlag-Rey M, Amador N, Sanchez H, Schlag J. 1997. Antisaccade performance predicted by neuronal activity in the supplementary eye field. Nature 390:398–401.

Shafiq-Antonacci R, Maruff P, Masters C, Currie J. 2003. Spectrum of saccade system function in Alzheimer disease. Arch Neurol 60:1272–1278.

Shehzad Z, Kelly AM, Reiss PT, Gee DG, Gotimer K, Uddin LQ, et al. 2009. The resting brain: unconstrained yet reliable. Cereb Cortex 19:2209–2229.

Smith SM, Fox PT, Miller KL, Glahn DC, Fox PM, Mackay CE, et al. 2009. Correspondence of the brain's functional architecture during activation and rest. Proc Natl Acad Sci USA 106:13040–13045.

Waites AB, Stanislavsky A, Abbott DF, Jackson GD. 2005. Effect of prior cognitive state on resting state networks measured with functional connectivity. Hum Brain Mapp 24:59–68.

Wang X, Han Z, He Y, Caramazza A, Song L, Bi Y. 2013. Where color rests: spontaneous brain activity of bilateral fusiform and lingual regions predicts object color knowledge performance. Neuroimage 76:252–263.

Werner CJ, Dogan I, Sab C, Mirzazade S, Shiefer J, Shah NJ, et al. 2014. Altered resting state connectivity in Huntington's disease. Hum Brain Mapp 35:2582–2593.

Zahran E, Aguirre GK, D'Esposito M. 1997. Empirical analyses of BOLD fMR statistics I spatially unsmoothed data collected under null-hypothesis conditions. Neuroimage 5:179–197.

Zuo QH, Zhu CZ, Yang Y, Zuo XN, Long Xy, Cao QJ, et al. 2008. An improved approach to detection of amplitude of low-frequency fluctuation (ALFF) for resting-state fMRI: fractional ALFF. J Neurosci Methods 172:137–141.

Zuo XN, Di Martino A, Kelly C, Shehzad ZE, Gee DG, Klein DF, et al. 2010a. The oscillating brain: complex and reliable. Neuroimage 49:1432–1445.

Zuo XN, Kelly C, Adelstein JS, Klein DF, Castellanos FX, Milham MP. 2010b. Reliable intrinsic connectivity networks: test-retest evaluation using ICA and dual regression approach. Neuroimage 49:2163–2177.

Address correspondence to:
Sharna D. Jamadar
Monash Biomedical Imaging
School of Psychological Sciences
Monash University
770 Blackburn Road
Clayton, VIC 3800
Australia

E-mail: sharna.jamadar@monash.edu